*SẽMA Journal*
*n$^o$ 54(2011), 47–64*

# A BRIEF SURVEY OF THE DISCONTINUOUS GALERKIN METHOD FOR THE BOLTZMANN-POISSON EQUATIONS

YINGDA CHENG*, IRENE M. GAMBA*, ARMANDO MAJORANA† AND CHI-WANG SHU‡

*Department of Mathematics and ICES, University of Texas at Austin,
†Dipartimento di Matematica e Informatica, Università di Catania,
‡Division of Applied Mathematics, Brown University

ycheng@math.utexas.edu, gamba@math.utexas.edu,
majorana@dmi.unict.it,shu@dam.brown.edu

**Abstract**

We are interested in the deterministic computation of the transients for the Boltzmann-Poisson system describing electron transport in semiconductor devices. The main difficulty of such computation arises from the very high dimensions of the model, making it necessary to use relatively coarse meshes and hence requiring the numerical solver to be stable and to have good resolution under coarse meshes. In this paper we give a brief survey of the discontinuous Galerkin (DG) method, which is a finite element method using discontinuous piecewise polynomials as basis functions and numerical fluxes based on upwinding for stability, for solving the Boltzmann-Poisson system. In many situations, the deterministic DG solver can produce accurate solutions with equal or less CPU time than the traditional DSMC (Direct Simulation Monte Carlo) solvers. In order to make the presentation more concise and to highlight the main ideas of the algorithm, we use a simplified model to describe the details of the DG method. Sample simulation results on the full Boltzmann-Poisson system are also given.

## A Introduction

The Boltzmann-Poisson (BP) system, which is a semiclassical description of electron flow in semiconductors, is an equation in six dimensions (plus time if the device is not in steady state) for a truly three dimensional device, and four dimensions for a one-dimensional device. This heavy computational cost explains why the BP

Received: September 15, 2010. Accepted: November 30, 2010.

Support from the Institute of Computational Engineering and Sciences and the University of Texas Austin is gratefully acknowledged. Research supported for the first author by NSF grant DMS-1016001. Research supported for the second author by NSF grant DMS-0807712 and DMS-0757450. Research supported for the third author by PRA 2009 Unict. Research supported for the fourth author by NSF grant DMS-0809086 and DOE grant DE-FG02-08ER25863.

system is traditionally simulated by the Direct Simulation Monte Carlo (DSMC) methods [25]. DSMC methods have the advantage that the increase in computational cost is not significant with the increase of dimensions. However, the simulation results are often noisy, and it is difficult to compute transient details (time dependent states), especially if the probability density function (*pdf*) is desired. In recent years, deterministic solvers to the BP system were considered in the literature, see for example [23, 28, 3, 2, 4, 5, 6, 24]. These methods provide accurate results which, in general, agree well with those obtained from DSMC simulations, sometimes at a comparable or even less computational time. Deterministic solvers have the distinct advantage in resolving transient details for the *pdf*. However, the main difficulty of the deterministic solvers arises from the very high dimensions of the model, making it necessary to use relatively coarse meshes and hence requiring the numerical solver to be stable and to have good resolution under coarse meshes. This can be challenging because under coarse meshes, for a convection dominated problem, the solution may contain high gradient (relative to the mesh) regions, which may lead to instability if care is not taken in the design of the algorithm.

One class of very successful numerical solvers for the deterministic solvers of the BP system is the weighted essentially non-oscillatory (WENO) finite difference scheme [4, 6]. The advantage of the WENO scheme is that it is relatively simple to code and very stable even on coarse meshes for solutions containing sharp gradient regions. However, the WENO finite difference method requires smooth meshes to achieve high order accuracy, hence it is not very flexible for adaptive meshes.

On the other hand, the Runge-Kutta discontinuous Galerkin (RKDG) method, which is a class of finite element methods originally devised to solve hyperbolic conservation laws [17, 16, 15, 14, 18], is a suitable alternative for solving the BP system. Using a completely discontinuous polynomial space for both the test and trial functions in the spatial variables and coupled with explicit and nonlinearly stable high order Runge-Kutta time discretization, the method has the advantage of flexibility for arbitrarily unstructured meshes, with a compact stencil, and with the ability to easily accommodate arbitrary *hp*-adaptivity. For more details about DG scheme for convection dominated problems, we refer to the review paper [20]. The DG method was later generalized to the local DG (LDG) method to solve the convection diffusion equation [19] and elliptic equations [1]. It is $L^2$ stable and locally conservative, which makes it particularly suitable to treat the Poisson equation.

In recent years, we have initialized a line of research to develop and implement the RKDG method, coupled with the LDG solution for the Poisson equation, for solving the full BP system, see [7, 8, 9, 10]. It is demonstrated through extensive numerical studies that the DG solver produces good resolution on relatively coarse meshes for the transient and steady state *pdf*, as well as various orders of moments and $I$-$V$ curves, which compare well with DSMC results. Our DG solver has the capability of handling full energy bands [10] that no other deterministic solver has been able to implement so far.

In this paper, we give a short survey of the DG solver for the full BP system. The emphasis is on the algorithm details, explained through a simplified model, and on sample simulation results to demonstrate the performance of the DG solver. The plan of the paper is as follows: in Section B, we will introduce the BP system and a simplified

model. In Section C, the DG scheme for this model will be presented. Section D includes some discussion and extensions of the algorithm. In Section E, we present some numerical results to show the performance of the scheme. Conclusions and future work are given in Section F. We collect some technical details of the implementation of the scheme in the Appendix.

## B The Boltzmann-Poisson system, and a simplified model

The evolution of the electron distribution function $f(\mathrm{t}, \mathbf{x}, \mathbf{k})$ in semiconductors, depending on the time $\mathrm{t}$, position $\mathbf{x}$ and electron wave vector $\mathbf{k}$, is governed by the Boltzmann transport equation (BTE) [26]

$$\frac{\partial f}{\partial \mathrm{t}} + \frac{1}{\hbar}\nabla_{\mathbf{k}}\,\varepsilon \cdot \nabla_{\mathbf{x}} f - \frac{q}{\hbar}\mathbf{E}\cdot\nabla_{\mathbf{k}} f = Q(f)\,, \tag{1}$$

where $\hbar$ is the reduced Planck constant, and $q$ denotes the positive elementary charge. The function $\varepsilon(\mathbf{k})$ is the energy of the considered crystal conduction band measured from the band minimum; according to the Kane dispersion relation, $\varepsilon$ is the positive root of

$$\varepsilon(1+\alpha\varepsilon) = \frac{\hbar^2 k^2}{2m^*}\,, \tag{2}$$

where $\alpha$ is the non-parabolicity factor and $m^*$ the effective electron mass. The electric field $\mathbf{E}$ is related to the doping density $N_D$ and the electron density $n$, which equals the zero-order moment of the electron distribution function $f$, by the Poisson equation

$$\nabla_{\mathbf{x}}\left[\varepsilon_r(\mathbf{x})\,\nabla_{\mathbf{x}} V\right] = \frac{q}{\varepsilon_0}\left[n(\mathrm{t},\mathbf{x}) - N_D(\mathbf{x})\right], \quad \mathbf{E} = -\nabla_{\mathbf{x}} V\,, \tag{3}$$

where $\varepsilon_0$ is the dielectric constant of the vacuum, $\varepsilon_r(\mathbf{x})$ labels the relative dielectric function depending on the semiconductor and $V$ is the electrostatic potential. For low electron densities, the collision operator $Q(f)$ is

$$Q(f)(\mathrm{t},\mathbf{x},\mathbf{k}) = \int_{\mathbb{R}^3}\left[S(\mathbf{k}',\mathbf{k}) f(\mathrm{t},\mathbf{x},\mathbf{k}') - S(\mathbf{k},\mathbf{k}') f(\mathrm{t},\mathbf{x},\mathbf{k})\right] d\mathbf{k}', \tag{4}$$

where $S(\mathbf{k}',\mathbf{k})$ is the kernel depending on the scattering mechanisms between electrons and phonons in the semiconductor.

In order to more clearly describe the details of the DG method, as well as to highlight the essential algorithm ingredients, we introduce a simplified model transport equation, which has the same characteristics as the full BP system. Thus, we consider the system

$$\frac{\partial u}{\partial t} + \frac{\partial}{\partial x}\left[a(v)\,u\right] + \frac{\partial}{\partial v}\left[b(v)\,\eta(t,x)\,u\right] = \int_{\mathbb{R}} K(v,v')\,u(t,x,v')\,dv' - \nu(v)\,u, \tag{5}$$

$$\frac{\partial}{\partial x}\left[\sigma(x)\,\frac{\partial \phi}{\partial x}\right] = \int_{\mathbb{R}} u(t,x,v')\,dv' - N_D(x),\ \eta(t,x) = -\frac{\partial \phi}{\partial x}. \tag{6}$$

Now, the unknown distribution function is $u$, which depends on time $t$, space coordinate $x \in [0,1]$ and the variable $v \in \mathbb{R}$ (velocity or energy). The functions $a$,

$b$, $\sigma$, $N_D$ and the kernel $K$ are given, and $K \geq 0$. The collision frequency $\nu$ is defined by the equation

$$\nu(v) = \int_{\mathbb{R}} K(v', v)\, dv' \tag{7}$$

which guarantees *mass conservation*.

## C The DG solver for the simplified model

We now discuss the DG solver for the model equations (5)-(6). The first step is to reduce the domain of the variable $v$ to a finite size. This can be justified because we expect a vanishing behavior of the unknown $u$ for large values of $v$. For rigorous justification, one could refer to the discussion in [12]. If $I$ is the finite interval used for the computation in the variable $v$, then we will replace $K(v, v')$ with $K(v, v')\, \chi_I(v)\, \chi_I(v')$, where $\chi_I$ is the characteristic function on $I$. The new collision frequency is redefined according Eq. (7). Therefore, this adjustment of the domain will not affect the mass conservation of the system.

For simplicity of discussion, we will use a simple rectangular grid to introduce the DG scheme, although the algorithm could be easily adjusted to accommodate general unstructured grids. For the domain $[0, 1] \times I$, we let

$$\Omega_{ik} = \left[x_{i-\frac{1}{2}},\, x_{i+\frac{1}{2}}\right] \times \left[v_{k-\frac{1}{2}},\, v_{k+\frac{1}{2}}\right]$$

where,

$$x_{i\pm\frac{1}{2}} = x_i \pm \frac{\Delta x_i}{2} \quad v_{k\pm\frac{1}{2}} = v_k \pm \frac{\Delta v_k}{2} \qquad (i = 1, 2, 3, ...N_x) \text{ and } (k = 1, 2, 3, ...N_v)\,.$$

We denote by $N_x$ and $N_v$ the number of intervals in the $x$ and $v$ direction, respectively.

The approximation space is defined as

$$V_h^\ell = \{v_h : (v_h)|_{\Omega_{ik}} \in P^\ell(\Omega_{ik})\}, \tag{8}$$

where $P^\ell(\Omega_{ik})$ is the set of all polynomials of degree at most $\ell$ on $\Omega_{ik}$. Notice that the polynomial degree $\ell$ can actually change from cell to cell ($p$-adaptivity), although in this paper it is kept as a constant for simplicity. The DG formulation for the simplified Boltzmann equation (5) would be: to find $u_h \in V_h^\ell$, such that

$$\begin{aligned}&\int_{\Omega_{ik}} (u_h)_t\, v_h\, dx\, dv - \int_{\Omega_{ik}} a(v) u_h\, (v_h)_x\, dx\, dv - \int_{\Omega_{ik}} b(v)\eta(t,x) u_h\, (v_h)_v\, dx\, dv \\ &+F_x^+ - F_x^- + F_v^+ - F_v^- = \int_{\Omega_{ik}} \left[\int_I K(v, v')\, u_h\, dv' - \nu(v)\, u_h\right] v_h\, dx\, dv \end{aligned} \tag{9}$$

for any test function $v_h \in V_h^\ell$. In (9),

$$F_x^+ = \int_{v_{k-\frac{1}{2}}}^{v_{k+\frac{1}{2}}} a(v)\, \breve{u}_h\, v_h^-(x_{i+\frac{1}{2}}, v) dv,$$

$$F_x^- = \int_{v_{k-\frac{1}{2}}}^{v_{k+\frac{1}{2}}} a(v)\, \check{u}_h\, v_h^+(x_{i-\frac{1}{2}}, v)dv,$$

$$F_v^+ = \int_{x_{i-\frac{1}{2}}}^{x_{i+\frac{1}{2}}} b(v_{k+\frac{1}{2}})\eta(t,x)\, \tilde{u}_h\, v_h^-(x, v_{k+\frac{1}{2}})dx,$$

$$F_v^- = \int_{x_{i-\frac{1}{2}}}^{x_{i+\frac{1}{2}}} b(v_{k-\frac{1}{2}})\eta(t,x)\, \tilde{u}_h\, v_h^-(x, v_{k-\frac{1}{2}})dx,$$

where the upwind numerical fluxes $\check{u}_h, \tilde{u}_h$ are chosen according to the following rules,

- if $a(v) \geq 0$ on the interval $[v_{k-\frac{1}{2}}, v_{k+\frac{1}{2}}]$, $\check{u}_h = u_h^-$; if $a(v) < 0$ on the interval $[v_{k-\frac{1}{2}}, v_{k+\frac{1}{2}}]$, $\check{u}_h = u_h^+$. Since $a(v)$ is a given function that does not depend on time, we will always be able to choose the grid such that $a(v)$ holds constant signs in each cell $[v_{k-\frac{1}{2}}, v_{k+\frac{1}{2}}]$.
- If $\int_{x_{i-\frac{1}{2}}}^{x_{i+\frac{1}{2}}} b(v_{k+\frac{1}{2}})\eta(t,x)dx > 0$, $\tilde{u}_h = u_h^-$; otherwise, $\tilde{u}_h = u_h^+$. Since the function $\eta$ depends on time, we can not choose a grid such that $b(v_{k+\frac{1}{2}})\eta(t,x)$ holds constant sign on each interval $[x_{i-\frac{1}{2}}, x_{i+\frac{1}{2}}]$. Here we relax the condition to look at the cell averages for the coefficient for easy implementation.

As for the Poisson equation (6), in the simple one-dimensional setting, one can use an exact Poisson solver or alternatively use a DG scheme designed for elliptic equations. Below we will describe the local DG methods [19] for (6) with Dirichlet boundary conditions. First, the Poisson equation is rewritten into the following form,

$$\begin{cases} q = \dfrac{\partial \phi}{\partial x} \\ \dfrac{\partial}{\partial x}(\sigma(x)q) = R(t,x) \end{cases} \tag{10}$$

where $R(t,x) = \int_I u_h(t,x,v')\,dv' - N_D(x)$ is a known function that can be computed at each time step once $u_h$ is solved from (9). The grid we use is $I_i = \left[x_{i-\frac{1}{2}},\, x_{i+\frac{1}{2}}\right]$, with $i = 1, \ldots, N_x$, which is consistent with the mesh for the Boltzmann equation. The approximation space is

$$W_h^\ell = \{v_h : (v_h)|_{I_i} \in P^\ell(I_i)\},$$

with $P^\ell(I_i)$ denoting the set of all polynomials of degree at most $\ell$ on $I_i$. The LDG scheme for (10) is given by: to find $q_h, \phi_h \in V_h^\ell$, such that

$$\int_{I_i} q_h v_h dx + \int_{I_i} \phi_h (v_h)_x dx - \hat{\phi}_h v_h^-(x_{i+\frac{1}{2}}) + \hat{\phi}_h v_h^+(x_{i-\frac{1}{2}}) = 0,$$

$$-\int_{I_i} \sigma(x) q_h (p_h)_x dx + \widehat{\sigma(x)q_h} p_h^-(x_{i+\frac{1}{2}}) - \widehat{\sigma(x)q_h} p_h^+(x_{i-\frac{1}{2}}) = \int_{I_i} R(t,x) p_h dx, \tag{11}$$

hold true for any $v_h, p_h \in W_h^\ell$. In the above formulation, the flux is chosen as follows, $\hat{\phi}_h = \phi_h^-$, $\widehat{\sigma(x)q_h} = (\sigma(x)q_h)^+ - [\phi_h]$, where $[\phi_h] = \phi_h^+ - \phi_h^-$. At $x = L$ we need

to flip the flux to $\hat{\phi}_h = \phi_h^+$, $\widehat{\sigma(x)q_h} = (\sigma(x)q_h)^- - [\phi_h]$ to adapt to the Dirichlet boundary conditions. Solving (11), we can obtain the numerical approximation of the electric potential $\phi_h$ and electric field $\eta_h = -q_h$ on each cell $I_i$. The so-called minimum dissipation LDG method [13] can also be used here.

To summarize, the DG-LDG algorithm advances from $t^n$ to $t^{n+1}$ in the following steps:

**Step 1** Compute $\int_I u_h(t, x, v')\, dv'$ and $R(t, x)$.

**Step 2** Solve the electric field $\eta_h(t, x)$ from (11).

**Step 3** Solve (9) and get a method of line ODE for $u_h$.

**Step 4** Evolve this ODE by proper time stepping from $t^n$ to $t^{n+1}$, if partial time step is necessary, then repeat Step 1 to 3 as needed.

The algorithm described above carries the essential ideas of those in [9] for the BP system. We include some of the technical details of the scheme in the Appendix for the reference of the readers.

## D Some considerations

In this section, we will review some aspects of the DG-BP solver developed in the literature and give an overview of some ongoing and future research directions.

### D.1 Mass conservation and positivity of the numerical solution

It is well known that the transport Boltzmann equation associated with the BP system conserves mass, and the initial value problem propagates positivity. In particular, it is essential that the numerical schemes preserve these physical properties of the system. In general, high order than one DG solvers as the one introduced in the previous section will not enjoy positivity. However it was shown in [12] that the semi-discrete DG scheme is positivity-preserving and stable for piecewise constants by arguments following an adaptation of the Crandall-Tartar lemma [22] to low order DG schemes, which states that any mass preserving, contracting linear first order operator is stable and monotone preserving. In addition, in [12] the authors also proposed a fully discrete positivity-preserving DG scheme for Vlasov-Boltzmann transport equation. They used a maximum-principle-satisfying limiter for conservation laws [32] and achieved a high order accurate DG solver that ensures the positivity of the numerical solution. A comparison study of the standard RKDG scheme against the positivity-preserving DG scheme has also been performed for the linear Boltzmann equation in [12].

Similarly for the DG-BP solver, clearly the following two properties will also hold, where the second one is a simple proof of positivity for the fully discrete scheme on piecewise constant basis functions.

**Property 1** *(Semi-discrete mass conservation) Under zero or periodic boundary conditions in the $x$ space, we have that*

$$\frac{d}{dt}\int_0^1 \int_I u_h dv dx = 0.$$

*Proof.* Plug in (9) with $v_h = 1$, and sum over all $i$, $k$, the conservation will follow.

**Property 2** *(Positivity for the first order scheme) Define* $A = \max a(v)$, $B = \max b(v)\eta(t,x)$ *and* $\bar{V} = \max \nu(v)$. *For first order DG scheme with piecewise constant approximation and forward Euler time discretization, if the CFL condition*

$$\lambda_1 A + \lambda_2 B + \triangle t \bar{V} \leq 1,$$

*is satisfied, where* $\lambda_1 = \frac{\triangle t}{\min_i \triangle x_i}$ *and* $\lambda_2 = \frac{\triangle t}{\min_k \triangle v_k}$, *then the DG scheme is monotone and will preserve the positivity of the numerical solution.*

*Proof.* Plug in (9) with $v_h = 1$, we have

$$\int_{\Omega_{ik}} (u_h)_t \, d\Omega + F_x^+ - F_x^- + F_v^+ - F_v^- = \int_{\Omega_{ik}} \left[ \int_I K(v,v') \, u_h \, dv' - \nu(v) \, u_h \right] d\Omega, \quad (12)$$

where

$$F_x^+ = \int_{v_{k-\frac{1}{2}}}^{v_{k+\frac{1}{2}}} a(v) \, \check{u}_h dv,$$

$$F_x^- = \int_{v_{k-\frac{1}{2}}}^{v_{k+\frac{1}{2}}} a(v) \, \check{u}_h dv,$$

$$F_v^+ = \int_{x_{i-\frac{1}{2}}}^{x_{i+\frac{1}{2}}} b(v_{k+\frac{1}{2}}) \eta(t,x) \, \tilde{u}_h dx,$$

$$F_v^- = \int_{x_{i-\frac{1}{2}}}^{x_{i+\frac{1}{2}}} b(v_{k-\frac{1}{2}}) \eta(t,x) \, \tilde{u}_h dx.$$

We assume $u_h = u_{ik}^n$ on $\Omega_{ik}$ at $t^n$, then

$$\begin{aligned} u_{ik}^{n+1} &= u_{ik}^n - \frac{\triangle t}{\triangle x_i \triangle v_k} \{ F_x^+ - F_x^- + F_v^+ - F_v^- + \int_{\Omega_{ik}} \int_I K(v,v') \, u_h \, dv' d\Omega \\ &\quad - \triangle x_i \int_{v_{k-\frac{1}{2}}}^{v_{k+\frac{1}{2}}} \nu(v) \, dv \, u_{ik}^n \}. \end{aligned}$$

As suggested by the definition for the numerical fluxes, if $a(v) \geq 0$ on the interval $[v_{k-\frac{1}{2}}, v_{k+\frac{1}{2}}]$, $\check{u}_h = u_h^-$, which implies $F_x^+ = (\int_{v_{k-\frac{1}{2}}}^{v_{k+\frac{1}{2}}} a(v) dv) \, u_{ik}^n$ and $F_x^- = (\int_{v_{k-\frac{1}{2}}}^{v_{k+\frac{1}{2}}} a(v) dv) \, u_{i-1,k}^n$. Otherwise, $F_x^+ = (\int_{v_{k-\frac{1}{2}}}^{v_{k+\frac{1}{2}}} a(v) dv) \, u_{i+1,k}^n$ and $F_x^- = (\int_{v_{k-\frac{1}{2}}}^{v_{k+\frac{1}{2}}} a(v) dv) \, u_{ik}^n$.

Similarly, if $\int_{x_{i-\frac{1}{2}}}^{x_{i+\frac{1}{2}}} b(v_{k+\frac{1}{2}}) \eta(t,x) dx > 0$, $\tilde{u}_h = u_h^-$, $F_v^+ = (\int_{x_{i-\frac{1}{2}}}^{x_{i+\frac{1}{2}}} b(v_{k+\frac{1}{2}}) \eta(t,x) \, dx) \, u_{ik}^n$ and $F_v^- = (\int_{x_{i-\frac{1}{2}}}^{x_{i+\frac{1}{2}}} b(v_{k+\frac{1}{2}}) \eta(t,x) \, dx) \, u_{i,k-1}^n$; otherwise, $F_v^+ = (\int_{x_{i-\frac{1}{2}}}^{x_{i+\frac{1}{2}}} b(v_{k+\frac{1}{2}}) \eta(t,x) \, dx) \, u_{i,k+1}^n$ and $F_v^- = (\int_{x_{i-\frac{1}{2}}}^{x_{i+\frac{1}{2}}} b(v_{k+\frac{1}{2}}) \eta(t,x) \, dx) \, u_{ik}^n$.

By taking derivative of all its variables, it is not difficult to verify that this is a monotone scheme if

$$\lambda_1 A + \lambda_2 B + \triangle t \bar{V} \leq 1.$$

Hence it will preserve the positivity of the numerical solution.

### D.2 Incorporation of full energy band models

The BP system introduced in Section B uses analytical band structures, which means the energy band function $\varepsilon(\mathbf{k})$ has been given explicitly. The analytical band makes use of the explicit dependence of the carrier energy on the quasimomentum, which significantly simplifies all expressions as well as implementation of these techniques. However, the physical details of the band structure are partly or totally ignored, which is unphysical when hot carriers in high-field phenomena are considered.

Full band models [21], on the other hand, can guarantee accurate physical pictures of the energy-band function. They are widely used in DSMC simulators, but only recently the Boltzmann transport equation was considered [31, 29], where approximate solutions were found by means of spherical harmonics expansion of the distribution function $f$. Since only a few terms of the expansion are usually employed, high order accuracy is not always achieved [27]. Recently in [10], the authors developed a DG code, which is the first deterministic code that can compute the full band model directly. The energy band is treated as a numerical input that can be obtained either by experimental data or the empirical pseudopotential method. The Dirac delta functions in the scattering kernels can be computed directly, based on the weak formulations of the PDE. The results in [10] for 1D devices have demonstrated the importance of using full band model when accurate description of hydromoments under large applied bias is desired. In a forthcoming manuscript [11], we will present a full implementation of the scheme with numerical bands as well as a thorough study of stability and error analysis.

In future work, we will extend the solver to include multi-carrier transport in devices such as P-N junctions. When modeling the P-N junctions, the carrier flows of both electrons and holes should be considered. The $pdf$ of electrons and holes will satisfy the following BTEs coupled with Poisson equation for the field,

$$\frac{\partial f_i}{\partial \mathrm{t}} + \frac{1}{\hbar}\nabla_{\mathbf{k}}\,\varepsilon_i \cdot \nabla_{\mathbf{x}} f_i \mp \frac{q}{\hbar}\mathbf{E}\cdot\nabla_{\mathbf{k}} f_i = Q_i(f) + R_i(f_e, f_h),\ i = e, h1, h2, h3,$$
$$[\varepsilon_r(\mathbf{x})\,\nabla_{\mathbf{x}} V] = \frac{q}{\varepsilon_0}\left[n_e(\mathrm{t},\mathbf{x}) - n_h(\mathrm{t},\mathbf{x}) - N_D(\mathbf{x}) + N_A(\mathbf{x})\right], \quad \mathbf{E} = -\nabla_{\mathbf{x}} V\,.$$

In the above equation, the subscript $e$ denotes electrons and $h1, h2, h3$ denote holes. One electron conduction band and three hole valence bands (heavy, light and split-off bands) need to be considered in order to have an accurate physical description. The $Q_i$ terms are the collision terms which have been introduced in Section 2 for electrons. For holes, those terms should include inter-band scattering as well. $R_i(f_e, f_h)$ is the recombination term. In this model, we need to solve for each carrier a Boltzmann transport equation and they are all coupled together through the Poisson equation for the electric field. It will be of particular interest to explore adaptive DG methods for solving this type of systems in order to reduce computational cost.

## E Numerical results for semiconductor devices

In this section, we will demonstrate the performance of DG schemes through the calculation for a 2D double gate MOSFET device. The schematic plot of the double

gate MOSFET device is given in Figure 1. The top and bottom shadowed region denotes the oxide-silicon region, whereas the rest is the silicon region.

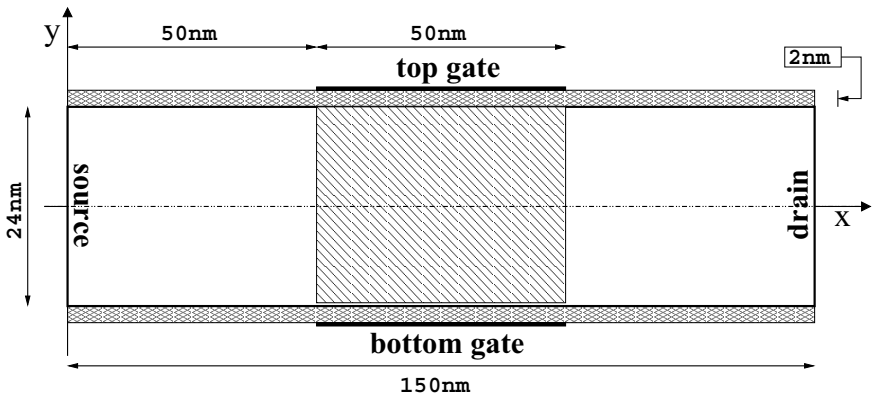


Figure 1: Schematic representation of a 2D double gate MOSFET device

Since the problem is symmetric about the x-axis, we will only need to compute for $y > 0$. At the source and drain contacts, we implement the same boundary condition as proposed in [6] to realize neutral charges. At the top and bottom of the computational domain (the silicon region), we impose the classical elastic specular boundary reflection. The electric potential $\Psi = 0$ at source, $\Psi = 1$ at drain and $\Psi = 0.5$ at gate. For the rest of boundaries, we impose homogeneous Neumann boundary condition. The relative dielectric constant in the oxide-silicon region is $\varepsilon_r = 3.9$, in the silicon region is $\varepsilon_r = 11.7$. The doping profile has been specified as follows: $N_D(x, y) = 5{\times}10^{17} cm^{-3}$ if $x < 50nm$ or $x > 100nm$, $N_D(x, y) = 2{\times}10^{15} cm^{-3}$ in the channel $50nm \leq x \leq 100nm$. All numerical results are obtained with a piecewise linear approximation space and second order TVD Runge-Kutta time stepping. We use a very coarse mesh, $24 \times 12$ grid in space, 24 points in $w$, 8 points in $\mu$ and 6 points in $\varphi$ in our calculation. In Figures 2 and 3, we show the results of the macroscopic quantities for the top part of the device when it is already at equilibrium.

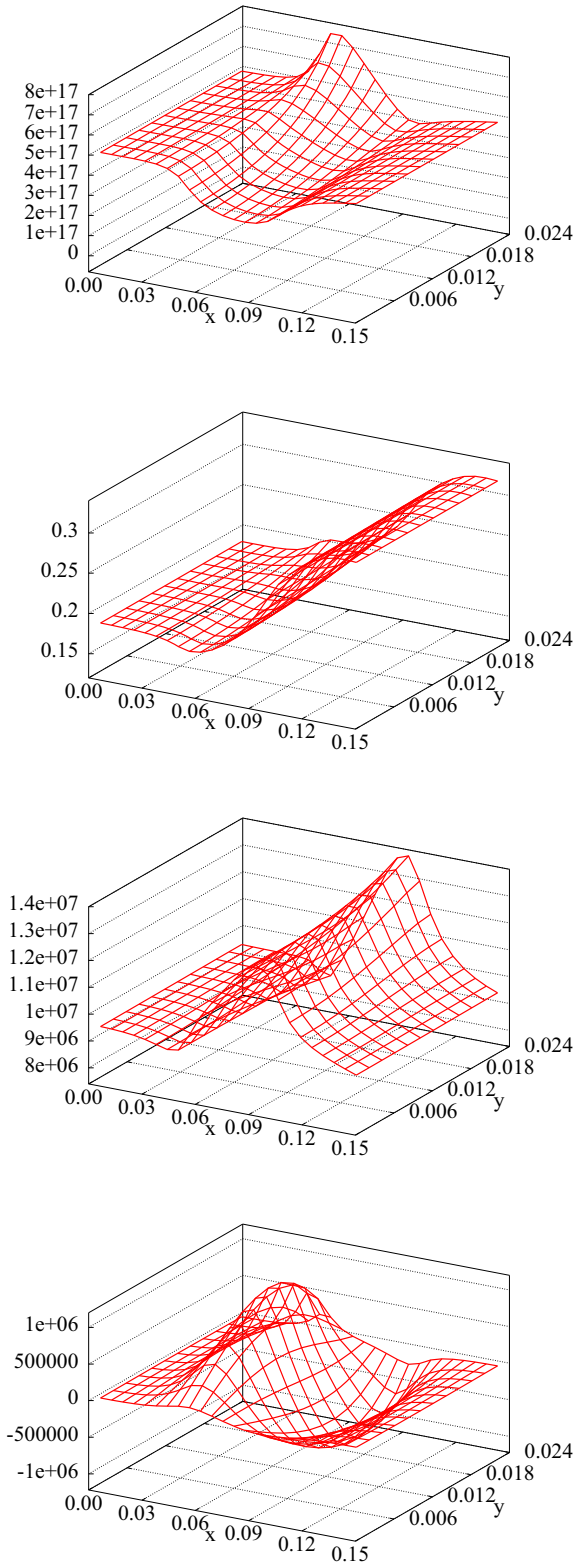


Figure 2: Macroscopic quantities of double gate MOSFET device at $t = 0.8$ps. Top left: density in $cm^{-3}$; top right: energy in $eV$; bottom left: x-component of velocity in $cm/s$; bottom right: y-component of velocity in $cm/s$. Solution reached steady state.

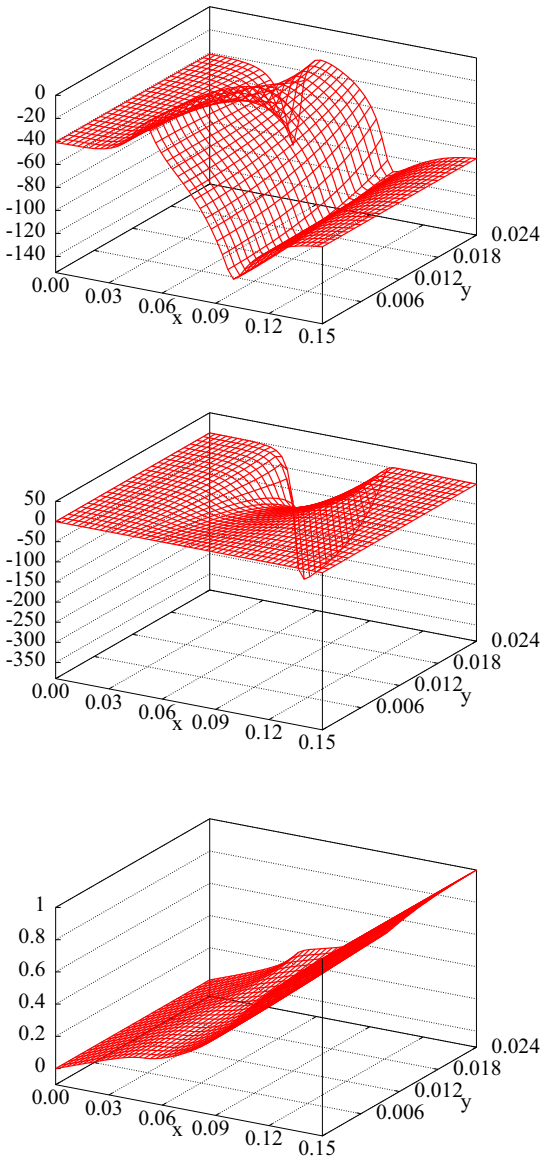


Figure 3: Macroscopic quantities of double gate MOSFET device at $t = 0.8$ps. Top left: x-component of electric field in $kV/cm$; top right: y-component of electric field in $kV/cm$; bottom: electric potential in $V$. Solution has reached steady state.

## F Concluding remarks and future work

In this paper, we present a brief survey of the current state-of-the-art of DG solvers for BP systems in semiconductor device simulations. We demonstrate the main ideas of the algorithm through a simplified model. We include some discussions of the properties and extensions of the schemes and show numerical results for the full BP system.

Deterministic solvers have recently gained growing attention in the field of semiconductor device modeling because of the guaranteed accuracy and noise-free simulation results they provide. However, the relative cost of this type of methods is still large especially when the dimension of the device is high. From the stand point of algorithm design and development, it will be interesting to explore ways to utilize fully the freedom of the DG framework such as *hp*-adaptivity. The DG schemes also provide an excellent platform for potential areas such as the hybridization of different level of models. For practical purposes, we will develop kinetic models and solvers to simulate nano-scale devices such as bipolar transistors, heterostructure bipolar transistors and solar cells in the future. Parallel implementation will also be an important component of our future research.

## References

[1] D. Arnold, F. Brezzi, B. Cockburn and L. Marini, *Unified analysis of discontinuous Galerkin methods for elliptic problems*, SIAM Journal on Numerical Analysis, 39 (2002), pp. 1749-1779.

[2] M.J. Caceres, J.A. Carrillo, I.M. Gamba, A. Majorana and C.-W. Shu, *Deterministic kinetic solvers for charged particle transport in semiconductor devices*, in Transport Phenomena and Kinetic Theory Applications to Gases, Semiconductors, Photons, and Biological Systems. C. Cercignani and E. Gabetta (Eds.), Birkhäuser (2006), pp. 151-171.

[3] J.A. Carrillo, I.M. Gamba, A. Majorana and C.-W. Shu, *A WENO-solver for 1D non-stationary Boltzmann-Poisson system for semiconductor devices*, Journal of Computational Electronics, 1 (2002), pp. 365-375.

[4] J.A. Carrillo, I.M. Gamba, A. Majorana and C.-W. Shu, *A direct solver for 2D non-stationary Boltzmann-Poisson systems for semiconductor devices: a MESFET simulation by WENO-Boltzmann schemes*, Journal of Computational Electronics, 2 (2003), pp. 375-380.

[5] J.A. Carrillo, I.M. Gamba, A. Majorana and C.-W. Shu, *A WENO-solver for the transients of Boltzmann-Poisson system for semiconductor devices. Performance and comparisons with Monte Carlo methods*, Journal of Computational Physics, 184 (2003), pp. 498-525.

[6] J.A. Carrillo, I.M. Gamba, A. Majorana and C.-W. Shu, *2D semiconductor device simulations by WENO-Boltzmann schemes: efficiency, boundary conditions and comparison to Monte Carlo methods*, Journal of Computational Physics, 214 (2006), pp. 55-80.

[7] Y. Cheng, I.M. Gamba, A. Majorana and C.-W. Shu, *Discontinuous Galerkin solver for the semiconductor Boltzmann equation*, SISPAD 07, T. Grasser and S. Selberherr, editors, Springer (2007), pp. 257-260.

[8] Y. Cheng, I. Gamba, A. Majorana and C.-W. Shu, *Discontinuous Galerkin solver for Boltzmann-Poisson transients*, Journal of Computational Electronics, 7 (2008), pp. 119-123.

[9] Y. Cheng, I. Gamba, A. Majorana and C.-W. Shu, *A discontinuous Galerkin solver for Boltzmann-Poisson systems for semiconductor devices*, Computer Methods in Applied Mechanics and Engineering, 198 (2009), pp. 3130-3150.

[10] Y. Cheng, I. Gamba, A. Majorana and C.-W. Shu, *A discontinuous Galerkin solver for full-band Boltzmann-Poisson models*, the Proceeding of IWCE 13, pp. 211-214, 2009.

[11] Y. Cheng, I.M. Gamba, A. Majorana and C.-W. Shu, *High order positive discontinuous Galerkin schemes for the Boltzmann-Poisson system with full bands*, in preparation.

[12] Y. Cheng, I.M. Gamba and J. Proft, *Positivity-preserving discontinuous Galerkin schemes for linear Vlasov-Boltzmann transport equations*, Mathematics of Computation, to appear.

[13] B. Cockburn and B. Dong, *An analysis of the minimal dissipation local discontinuous Galerkin method for convection-diffusion problems*, Journal of Scientific Computing, 32 (2007), pp. 233-262.

[14] B. Cockburn, S. Hou and C.-W. Shu, *The Runge-Kutta local projection discontinuous Galerkin finite element method for conservation laws IV: the multidimensional case*, Mathematics of Computation, 54 (1990), pp. 545-581.

[15] B. Cockburn, S.-Y. Lin and C.-W. Shu, *TVB Runge-Kutta local projection discontinuous Galerkin finite element method for conservation laws III: one dimensional systems*, Journal of Computational Physics, 84 (1989), pp. 90-113.

[16] B. Cockburn and C.-W. Shu, *TVB Runge-Kutta local projection discontinuous Galerkin finite element method for conservation laws II: general framework*, Mathematics of Computation, 52 (1989), pp. 411-435.

[17] B. Cockburn and C.-W. Shu, *The Runge-Kutta local projection P1-discontinuous Galerkin finite element method for scalar conservation laws*, Mathematical Modelling and Numerical Analysis, 25 (1991), pp. 337-361.

[18] B. Cockburn and C.-W. Shu, *The Runge-Kutta discontinuous Galerkin method for conservation laws V: multidimensional systems*, Journal of Computational Physics, 141 (1998), pp. 199-224.

[19] B. Cockburn and C.-W. Shu, *The local discontinuous Galerkin method for time-dependent convection-diffusion systems*, SIAM Journal on Numerical Analysis, 35 (1998), pp. 2440-2463.

[20] B. Cockburn and C.-W. Shu, *Runge-Kutta discontinuous Galerkin methods for convection-dominated problems*, Journal of Scientific Computing, 16 (2001), pp. 173-261.

[21] M. L. Cohen and J. Chelikowsky. *Electronic Structure and Optical Properties of Semiconductors*. Springer-Verlag, 1989.

[22] M. G. Crandall and L. Tartar. *Some relations between nonexpansive and order preserving mappings*, Proc. Amer. Math. Soc., 78 (1980), pp. 385-390.

[23] E. Fatemi and F. Odeh, *Upwind finite difference solution of Boltzmann equation applied to electron transport in semiconductor devices*, Journal of Computational Physics, 108 (1993), pp. 209-217.

[24] M. Galler and A. Majorana, *Deterministic and stochastic simulation of electron transport in semiconductors*, Bulletin of the Institute of Mathematics, Academia Sinica (New Series), 6th MAFPD (Kyoto) special issue Vol. 2 (2007), No. 2, pp. 349-365.

[25] C. Jacoboni and P. Lugli, *The Monte Carlo Method for Semiconductor Device Simulation*, Spring-Verlag: Wien-New York, 1989.

[26] M. Lundstrom, *Fundamentals of Carrier Transport*, Cambridge University Press: Cambridge, 2000.

[27] A. Majorana, *A comparison between bulk solutions to the Boltzmann equation and the spherical harmonic model for silicon devices*, in *Progress in Industrial Mathematics at ECMI 2000 - Mathematics in Industry*, 1 (2002), pp. 169-173.

[28] A. Majorana and R. Pidatella, *A finite difference scheme solving the Boltzmann Poisson system for semiconductor devices*, Journal of Computational Physics, 174 (2001), pp. 649-668.

[29] S. Smirnov and C. Jungemann, *A full band deterministic model for semiclassical carrier transport in semiconductors*, Journal of Applied Physics, 99 (1988), 063707.

[30] K. Tomizawa, *Numerical Simulation of Submicron Semiconductor Devices*, Artech House: Boston, 1993.

[31] M. C. Vecchi, D. Ventura, A. Gnudi and G. Baccarani. *Incorporating full band-structure effects in spherical harmonics expansion of the Boltzmann transport equation*, in *Proceedings of NUPAD V Conference*, 8 (1994), pp. 55-58.

[32] X. Zhang and C.-W. Shu, *On maximum-principle-satisfying high order schemes for scalar conservation laws*, Journal of Computational Physics, 229 (2010), pp. 3091-3120.

[33] J.M. Ziman, *Electrons and Phonons. The Theory of Transport Phenomena in Solids*, Oxford University Press: Oxford, 2000.

## G Appendix

In this appendix, we will include some of the implementation details of the proposed DG algorithm for the full BP system.

For a silicon device, the collision operator (4) takes into account acoustic deformation potential and optical intervalley scattering [30, 33]. For low electron densities, it reads

$$Q(f)(\mathrm{t},\mathbf{x},\mathbf{k}) = \int_{\mathbb{R}^3} \left[S(\mathbf{k}',\mathbf{k}) f(\mathrm{t},\mathbf{x},\mathbf{k}') - S(\mathbf{k},\mathbf{k}') f(\mathrm{t},\mathbf{x},\mathbf{k})\right] d\mathbf{k}' \tag{13}$$

with the scattering kernel

$$\begin{aligned} S(\mathbf{k},\mathbf{k}') \;&=\; (n_q+1)\, K\, \delta(\varepsilon(\mathbf{k}') - \varepsilon(\mathbf{k}) + \hbar\omega_p) \\ &\quad + n_q\, K\, \delta(\varepsilon(\mathbf{k}') - \varepsilon(\mathbf{k}) - \hbar\omega_p) + K_0\, \delta(\varepsilon(\mathbf{k}') - \varepsilon(\mathbf{k})) \end{aligned} \tag{14}$$

and $K$ and $K_0$ being constant for silicon. The symbol $\delta$ indicates the usual Dirac distribution and $\omega_p$ is the constant phonon frequency. Moreover,

$$n_q = \left[\exp\left(\frac{\hbar\omega_p}{k_B T_L}\right) - 1\right]^{-1}$$

is the occupation number of phonons, $k_B$ the Boltzmann constant and $T_L$ the constant lattice temperature. In Table 1, we list the physical constants for a typical silicon device.

| | | |
|---|---|---|
| $m^* = 0.32\, m_e$ | $T_L = 300\, K$ | $\hbar\omega_p = 0.063\, eV$ |
| $K = \dfrac{(D_t K)^2}{8\pi^2 \varrho\, \omega_p}$ | $D_t K = 11.4\, eV\ \text{Å}^{-1}$ | $\varrho = 2330\,\mathrm{kg\,m^{-3}}$ |
| $K_0 = \dfrac{k_B T_L}{4\pi^2 \hbar\, v_0^2\, \varrho}\, \Xi_d^2$ | $\Xi_d = 9\, eV$ | $v_0 = 9040\,\mathrm{m\,s^{-1}}$ |
| $\varepsilon_r = 11.7$ | $\alpha = 0.5\, eV$ | |

*Table 1. Values of the physical parameters*

For the numerical treatment of the Boltzmann-Poisson system (1), (3), it is convenient to introduce suitable dimensionless quantities and variables. Typical values for length, time and voltage are $\ell_* = 10^{-6}\, m$, $t_* = 10^{-12}\, s$ and $V_* = 1\,\mathrm{Volt}$, respectively. Thus, we define the dimensionless variables

$$(x,y,z) = \frac{\mathbf{x}}{\ell_*}, \quad t = \frac{\mathrm{t}}{t_*}, \quad \Psi = \frac{V}{V_*}, \quad (E_x,E_y,E_z) = \frac{\mathbf{E}}{E_*}$$

with $E_* = 0.1\, V_*\, \ell_*^{-1}$ and

$$E_x = -c_v \frac{\partial \Psi}{\partial x}, \quad E_y = -c_v \frac{\partial \Psi}{\partial y}, \quad c_v = \frac{V_*}{\ell_* E_*}.$$

In correspondence to [28] and [5], we perform a coordinate transformation for $\mathbf{k}$ according to

$$\mathbf{k} = \frac{\sqrt{2m^* k_B T_L}}{\hbar} \sqrt{w(1+\alpha_K w)} \left( \mu, \sqrt{1-\mu^2}\cos\varphi, \sqrt{1-\mu^2}\sin\varphi \right), \qquad (15)$$

where the new independent variables are the dimensionless energy $w = \dfrac{\varepsilon}{k_B T_L}$, the cosine of the polar angle $\mu$ and the azimuth angle $\varphi$ with $\alpha_K = k_B T_L \alpha$. The main advantage of the generalized spherical coordinates (15) is the easy treatment of the Dirac distribution in the kernel (14) of the collision term. In fact, this procedure enables us to transform the integral operator (4) with the not regular kernel $S$ into an integral-difference operator, as shown in the following.

We are interested in studying two-dimensional problems in real space; this requires the full three-dimensional $\mathbf{k}$-space. Therefore, it is useful to consider the new unknown function $\Phi$ related to the electron distribution function via

$$\Phi(t,x,y,w,\mu,\varphi) = s(w) f(\mathrm{t},\mathbf{x},\mathbf{k})\big|_{\mathrm{t}=t_* t\,,\,\mathbf{x}=\ell_*(x,y,z)\,,\,\mathbf{k}=\frac{\sqrt{2m^* k_B T_L}}{\hbar}\sqrt{w(1+\alpha_K w)}\,\ldots}\,,$$

where

$$s(w) = \sqrt{w(1+\alpha_K w)}(1+2\alpha_K w), \qquad (16)$$

is proportional to the Jacobian of the change of variables (15) and, apart from a dimensional constant factor, to the density of states. This allows us to write the free streaming operator of the dimensionless Boltzmann equation in a conservative form, which is appropriate for applying standard numerical schemes used for hyperbolic partial differential equations. Due to the symmetry of the problem and of the collision operator, we have

$$\Phi(t,x,y,w,\mu,2\pi-\varphi) = \Phi(t,x,y,w,\mu,\varphi)\,. \qquad (17)$$

Straightforward but cumbersome calculations end in the following transport equation for $\Phi$:

$$\frac{\partial\Phi}{\partial t} + \frac{\partial}{\partial x}(g_1\Phi) + \frac{\partial}{\partial y}(g_2\Phi) + \frac{\partial}{\partial w}(g_3\Phi) + \frac{\partial}{\partial \mu}(g_4\Phi) + \frac{\partial}{\partial \varphi}(g_5\Phi) = C(\Phi)\,. \qquad (18)$$

The functions $g_i$ $(i = 1,2,..,5)$ in the advection terms depend on the independent variables $w$, $\mu$, $\varphi$ as well as on time and position via the electric field. They are given

by

$$
\begin{aligned}
g_1(\cdot) &= c_x \frac{\mu\sqrt{w(1+\alpha_K w)}}{1+2\alpha_K w}\,,\\
g_2(\cdot) &= c_x \frac{\sqrt{1-\mu^2}\sqrt{w(1+\alpha_K w)}\cos\varphi}{1+2\alpha_K w}\,,\\
g_3(\cdot) &= -2c_k \frac{\sqrt{w(1+\alpha_K w)}}{1+2\alpha_K w}\left[\mu\, E_x(t,x,y) + \sqrt{1-\mu^2}\cos\varphi\, E_y(t,x,y)\right]\,,\\
g_4(\cdot) &= -c_k \frac{\sqrt{1-\mu^2}}{\sqrt{w(1+\alpha_K w)}}\left[\sqrt{1-\mu^2}\, E_x(t,x,y) - \mu\cos\varphi\, E_y(t,x,y)\right]\,,\\
g_5(\cdot) &= c_k \frac{\sin\varphi}{\sqrt{w(1+\alpha_K w)}\sqrt{1-\mu^2}}\, E_y(t,x,y)
\end{aligned}
$$

with

$$
c_x = \frac{t_*}{\ell_*}\sqrt{\frac{2\,k_B T_L}{m^*}} \quad\text{and}\quad c_k = \frac{t_* q E_*}{\sqrt{2m^* k_B T_L}}\,.
$$

The right hand side of (18) is the integral-difference operator

$$
\begin{aligned}
&C(\Phi)(t,x,y,w,\mu,\varphi) = s(w)\left\{c_0\int_0^\pi d\varphi'\int_{-1}^1 d\mu'\,\Phi(t,x,y,w,\mu',\varphi')\right.\\
&\left.+\int_0^\pi d\varphi'\int_{-1}^1 d\mu'\,[c_+\Phi(t,x,y,w+\gamma,\mu',\varphi') + c_-\Phi(t,x,y,w-\gamma,\mu',\varphi')]\right\}\\
&-2\pi[c_0 s(w) + c_+ s(w-\gamma) + c_- s(w+\gamma)]\Phi(t,x,y,w,\mu,\varphi)\,,
\end{aligned}
$$

where

$$
(c_0,c_+,c_-) = \frac{2m^*\,t_*}{\hbar^3}\sqrt{2\,m^*\,k_B T_L}\,(K_0,(n_q+1)K,n_q K)\,,\quad \gamma = \frac{\hbar\omega_p}{k_B T_L}
$$

are dimensionless parameters. We remark that the $\delta$ distributions in the kernel $S$ have been eliminated which leads to the shifted arguments of $\Phi$. The parameter $\gamma$ represents the jump constant corresponding to the quantum of energy $\hbar\omega_p$. We have also taken into account (17) in the integration with respect to $\varphi'$.

In terms of the new variables the electron density becomes

$$
n(t_*t,\ell_*x,\ell_*y) = \int_{\mathbb{R}^3} f(t_*t,\ell_*x,\ell_*y,\mathbf{k})\,d\mathbf{k} = \left(\frac{\sqrt{2\,m^*k_B T_L}}{\hbar}\right)^3\rho(t,x,y)\,,
$$

where

$$
\rho(t,x,y) = \int_0^{+\infty} dw\int_{-1}^1 d\mu\int_0^\pi d\varphi\,\Phi(t,x,y,w,\mu,\varphi)\,. \tag{19}
$$

Further hydrodynamical variables are the dimensionless $x$-component of the velocity

$$
\frac{\displaystyle\int_0^{+\infty} dw\int_{-1}^1 d\mu\int_0^\pi d\varphi\, g_1(w)\,\Phi(t,x,y,w,\mu,\varphi)}{\rho(t,x,t)}\,,
$$

and the dimensionless energy

$$\frac{\displaystyle\int_0^{+\infty} dw \int_{-1}^{1} d\mu \int_0^{\pi} d\varphi \, w \, \Phi(t,x,y,w,\mu,\varphi)}{\rho(t,x,t)} \, .$$

Using the new dimensionless variables, Poisson equation becomes

$$\frac{\partial}{\partial x}\left(\varepsilon_r \frac{\partial \Psi}{\partial x}\right) + \frac{\partial}{\partial y}\left(\varepsilon_r \frac{\partial \Psi}{\partial y}\right) = c_p \left[\rho(t,x,t) - \mathcal{N}_D(x,y)\right] \tag{20}$$

with

$$\mathcal{N}_D(x,y) = \left(\frac{\sqrt{2\, m^* k_B T_L}}{\hbar}\right)^{-3} N_D(\ell_* x, \ell_* y) \text{ and } c_p = \left(\frac{\sqrt{2\, m^* k_B T_L}}{\hbar}\right)^{3} \frac{\ell_*^2 q}{\varepsilon_0} \, .$$

To solve the dimensionless Boltzmann-Poisson system, we need the initial conditions for $\Phi$ and boundary conditions both for $\Phi$ and $\Psi$. These depend on the geometry of the device and on the problem. In the $(w, \mu, \varphi)$-space, no boundary condition is necessary. In fact,

- at $w = 0$, $g_3 = 0$. At $w = w_{\text{max}}$, $\Phi$ is assumed machine zero;
- at $\mu = \pm 1$, $g_4 = 0$;
- at $\varphi = 0, \pi$, $g_5 = 0$,

so at those boundaries, the numerical flux always vanishes, hence no ghost point is necessary for the DG method.